

CONTOUR DETECTION BY SURROUND INHIBITION IN THE CIRCULAR HARMONIC FUNCTIONS DOMAIN

*Giuseppe Papari**, *Patrizio Campisi***, *Nicolai Petkov**, and *Alessandro Neri***

*Institute of Mathematics and Computing Science, University of Groningen,
P. O. Box 800, 9700 AV Groningen, The Netherlands
phone: + (31) 50 3633939, fax: + (31) 50 3633800, email: (g.papari, petkov)@cs.rug.nl
www.cs.rug.nl

**Dipartimento di Elettronica Applicata, Univesità degli Studi "Roma TRE",
Via della Vasca Navale, 84, I-00146 Roma, Italy
phone: + (39)06.5517.7064, fax: + (39)06.55177026, email: (campisi, neri)@uniroma3.it
www.comlab.ele.uniroma3.it

ABSTRACT

Standard edge detectors react to all not negligible luminance changes in an image, irrespective whether they are originated by object contours or by texture (e.g. grass, foliage, waves, etc.). Texture edges are often stronger than object contours, thus standard edge detectors fail in isolating object contours from texture. We propose a multiresolution contour detector, operating in the Circular Harmonic Function domain and motivated by biological principles. At each scale, texture is suppressed by using a bilateral surround inhibition process, applied after non-maxima suppression. The binary contour map is obtained by a contour-oriented thresholding algorithm, proved to be more effective than the classical hysteresis thresholding used in the Canny edge detector. Robustness to noise is achieved by a Bayesian gradient estimation.

1. INTRODUCTION

The last two decades have seen a flourishing development in the field of edge detection. Examples of edge detectors are operators incorporating linear filtering [1], local orientation analysis [2], fitting of analytical models to the image data [3], and local energy [4]. In object recognition tasks, these methods suffer the drawback of reacting to all luminance changes, irrespective of their origin: object contours or texture. Moreover, in many cases the gradient magnitude is stronger on textured areas than on object contours. Since the Human Visual System (HVS) can easily make such a distinction, we take into account some aspects of the HVS to improve the mentioned selectivity property of the contour extraction.

For instance, psychophysical studies show that the HVS processes low and high spatial frequencies with different latencies [5]: low frequencies are processed in the first 0.1 ÷ 0.3s after an image is projected on the retina, thus only the general morphology is perceived; in the subsequent stage, also the information in higher spatial frequencies is processed and details are perceived. This suggests that contour detection should be performed in a multiresolution framework [6], [7].

Other psychophysical and neurophysiological studies reveal the existence of a phenomenon called surround suppression — see e.g. [8], [9] and the references therein — leading to reduction of the response of an orientation selective neuron to an oriented stimulus, when it is surrounded by other similar stimuli. In [9] it is suggested that the biological utility of surround suppression is contour enhancement in natural images rich in background texture.

Contour detection becomes an even more challenging task when applied to noisy images. To make contour detection robust to noise,

we introduce a Bayesian denoising step that deploys the optimal Minimum Mean Square Error (MMSE) estimator of the gradient in additive noise. According to recent statistical studies on natural images [10], parametric probabilistic models based on Gaussian Scale Mixtures (GSM) are adopted for both signal and noise edge features. This assumption leads to a closed form of the estimator.

In this paper we combine multiresolution analysis, optimal Bayesian MMSE estimation of the gradient, and surround suppression. For multiresolution analysis we use Circular Harmonic Functions (CHF) [11]. The image contours are extracted at different resolutions and the obtained binary maps are combined by the logic AND operator. This approach relies on the assumption that contours are present at each resolution, while texture details are present only at the finest ones. In order to counteract the effect of noise, at each scale we perform noise reduction by using an optimal Bayesian MMSE estimation of the gradient, followed by a biologically motivated surround inhibition step.

2. CIRCULAR HARMONIC FUNCTIONS

In this Section, CHFs are introduced and some considerations on their relevance in modelling some aspects of the early stages of the HVS are detailed. Given an image $I(x, y) \in L^2(\mathbb{R}^2)$, let

$I_p(r, \theta) = I(\xi_1 + r \cos \theta, \xi_2 + r \sin \theta)$ be its representation in a polar coordinate system (r, θ) , centered at point (ξ_1, ξ_2) , where

$r = \sqrt{(x - \xi_1)^2 + (y - \xi_2)^2}$ and $\theta = \arctan \frac{y - \xi_2}{x - \xi_1}$. Then, given a

weighting function $w_{RTP}(r)$, the *radial tomographic projection* (RTP) is defined as follows:

$$RTP_\theta(\xi_1, \xi_2) = \int_0^\infty w_{RTP}(r) I_p(r, \theta) dr \quad (1)$$

Since $RTP_\theta(\xi_1, \xi_2)$ is periodic with respect to θ it can be decomposed into a Fourier series as follows

$$RTP_\theta(\xi_1, \xi_2) = \sum_{n=-\infty}^{+\infty} RTP^{(n)}(\xi_1, \xi_2) e^{jn\theta} \quad (2)$$

with

$$RTP^{(n)}(\xi_1, \xi_2) = \frac{1}{2\pi} \int_0^{2\pi} RTP_\theta(\xi_1, \xi_2) e^{-jn\theta} d\theta \quad (3)$$

being the n -th radial coefficient of the RTP. The radial coefficient

$RTP^{(n)}(\xi_1, \xi_2)$ is related to the image $I(x, y)$ by the following convolution

$$RTP^{(n)}(\xi_1, \xi_2) = I(\xi_1, \xi_2) * \frac{w_{RTP} \left(\sqrt{\xi_1^2 + \xi_2^2} \right) e^{-jn \arctan \frac{\xi_2}{\xi_1}}}{2\pi \sqrt{\xi_1^2 + \xi_2^2}} \quad (4)$$

The functions

$$\psi^{(n)}(r, \theta) = h_n(r) e^{-jn\theta} \quad (5)$$

where $2\pi h_n(r) = \frac{w_{RTP}(r)}{r}$, are known in the literature as circular

harmonic functions (CHF) of order n with radial profile $h_n(r)$. The CHF transform generates complex images, where the magnitude reveals the presence of specific features, and the phase is proportional to their orientation. In general, the n -th order CHF is tuned to the fundamental harmonics of n -fold angular symmetric patterns, corresponding to edges ($n=1$), lines ($n=2$), forks ($n=3$), crosses ($n=4$) and so on. It is worth noting that the polar separability property that characterizes the circular harmonic filters in the spatial domain holds also in the frequency domain.

For the application pursued in this paper, let us consider the following polar separable functions:

$$\psi_{\sigma_i}^{(n)}(r, \theta) = \left(\frac{r}{\sigma_i} \right)^n e^{-(r^2/\sigma_i^2)} e^{-jn\theta} \quad (6)$$

known as ‘‘marginal’’ Hermite filters ($n=0,1,2,3,\dots$).

Fig.1 shows the outputs of the ‘‘marginal’’ Hermite filters for a synthetic test image and demonstrates the CHF’s abilities to highlight edges, lines, forks, and crosses when using the orders $n=1$, $n=2$, $n=3$, and $n=4$, respectively. For the purpose of this study, in the following we use only CHF’s of order $n=1$.



Figure 1 - From left to right: test image, magnitude of the outputs of the ‘‘marginal’’ Hermite filters of order $n=1, 2, 3, 4$.

3. MULTIREOLUTION CONTOUR DETECTOR

As well known from multiresolution analysis [11], the outputs of coarse scale edge detectors do not contain much texture (Fig. 2a), but contours are smoothed and shifted [12] and non-maxima suppression destroys the junctions. At fine scales, contours are well detailed (Fig 2b), but much texture is present. The advantages given of different resolutions can be exploited by selecting, from the binary edge map obtained at a fine scale, only those edge pixels being close enough to edge pixels present in a map obtained at a coarse scale. The result contains well located contours but does not contain texture edges, since they are not present at the coarse scale (Fig. 2c). We apply this principle to the binary outputs of N Scale Dependant Contour Enhancers (SDCE) each of which is responsible for a different resolution (Fig. 3). The design of a SDCE is described in Section 4.

Specifically, let us consider a given image $I(x, y)$ and its observed version $I^Z(x, y)$ corrupted by additive independent observation noise $Z(x, y)$. First, the noisy image undergoes a multiresolution analysis by taking the magnitudes of the results of convolutions with CHF functions $\psi_{\sigma_i}^{(n)}(x, y)$ of order $n=1$ of different resolutions σ_i , $i=0, 1, \dots, N-1$:

$$I_{\sigma_i}^Z(x, y) = \left| I^Z(x, y) * \psi_{\sigma_i}^{(1)}(x, y) \right|. \quad (7)$$

Then binary maps b_i are computed by applying the SDCE operator described in Section 4:

$$b_i = SDCE_{\sigma_i} \left\{ I_{\sigma_i}^Z \right\} \quad (8)$$

The binary maps obtained at different scales are combined as shown in Fig. 3. First, we apply morphological dilation to all binary maps but the one that corresponds to the finest scale:

$$b_{k,DIL} = b_k \oplus D_3, \quad k=2, \dots, N-1 \quad (9)$$

where we use a disk D_3 of radius three pixels as a structuring element. The final output is given by the logic AND of the binary maps at all resolutions:

$$b_{out} = b_0(x, y) \cdot \prod_{k=1}^{N-1} b_{k,DIL}(x, y) \quad (10)$$

Morphological dilation compensates the shifting at the coarser resolutions and restores the junctions.

4. SCALE DEPENDANT CONTOUR ENHANCER

The proposed Scale Dependant Contour Enhancer (SDCE) is depicted in Fig. 4. The first processing step is Bayesian denoising (Section 4.1). Then non-maxima suppression and surround inhibition are performed (Section 4.2), followed by binarization (Section 4.3).

4.1 Bayesian denoising

Our goal is to find the optimal estimator $\tilde{I}_\sigma = \hat{\mathbf{a}}(\mathbf{z})$ for the unknown vector $\mathbf{a} = I_\sigma$, when a noisy version $\mathbf{z} = I_\sigma^Z = I_\sigma + Z_\sigma$ is observed. As well known from the Bayesian estimation theory, the MMSE estimator is given by:

$$\hat{\mathbf{a}}(\mathbf{z}) = \frac{p_{z|\mathbf{a}}(\mathbf{z}|\mathbf{a}) p_{\mathbf{a}}(\mathbf{a})}{\int p_{z|\mathbf{a}}(\mathbf{z}|\mathbf{a}) p_{\mathbf{a}}(\mathbf{a}) d\mathbf{a}} \quad (11)$$

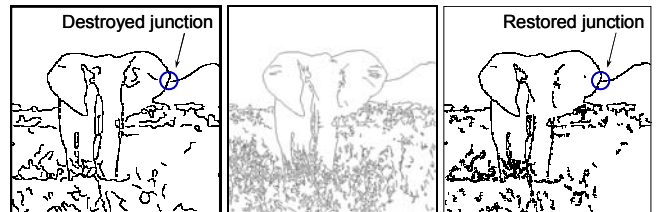


Figure 2 - Binary maps obtained from the outputs of a CHF filter for: (a) a coarse scale, (b) a fine scale, (c) a combination of the two scales by morphological dilation and logic AND.

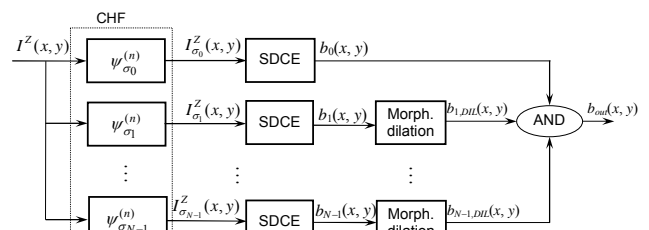


Figure 3 – Multiscale contour detector.

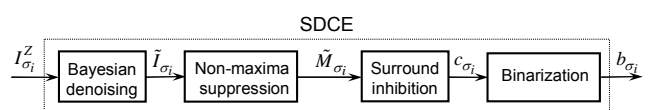


Figure 4 - Single scale contour detector.

According to recent statistical studies on natural images [11], both $p_{\mathbf{a}}(\mathbf{a})$ and $p_{\mathbf{z}|\mathbf{a}}(\mathbf{z}|\mathbf{a})$ are assumed GSM, with covariance matrices \mathbf{A}_i and \mathbf{N}_k for the signal and the noise, respectively:

$$\begin{cases} p_{\mathbf{a}}(\mathbf{a}) = \sum_{i=1}^{K_1} \lambda_i \mathcal{N}_2(\mathbf{a}, \mathbf{0}, \mathbf{A}_i) \\ p_{\mathbf{z}|\mathbf{a}}(\mathbf{z}|\mathbf{a}) = \sum_{k=1}^{K_2} \beta_k \mathcal{N}_2(\mathbf{z}, \mathbf{a}, \mathbf{N}_k) \end{cases}, \quad \sum_{i=1}^{K_1} \lambda_i = \sum_{k=1}^{K_2} \beta_k = 1 \quad (12)$$

where:

$$\mathcal{N}_2(\xi, \boldsymbol{\mu}, \mathbf{R}) = \frac{1}{2\pi \det \mathbf{R}} \exp\left[-\frac{1}{2}(\xi - \boldsymbol{\mu})^T \mathbf{R}^{-1}(\xi - \boldsymbol{\mu})\right] \quad (13)$$

By substituting eq. (12) in eq. (11), we can find the following closed expression for the optimal MMSE estimator:

$$\hat{\mathbf{a}}(\mathbf{z}) = \frac{\sum_{i,k} \lambda_i \beta_k \mathcal{N}_2(\mathbf{z}, \mathbf{0}, \mathbf{A}_i + \mathbf{N}_k) \mathbf{A}_i (\mathbf{A}_i + \mathbf{N}_k)^{-1} \mathbf{z}}{\sum_{i,k} \mathcal{N}_2(\mathbf{z}, \mathbf{0}, \mathbf{A}_i + \mathbf{N}_k)}. \quad (14)$$

The nonlinearity defined by eq. (14), applied to each pixel of I_{σ}^Z , gives the optimal MMSE estimation \tilde{I}_{σ} of I_{σ} . It is worth pointing out that the best *linear* MMSE estimate would give the Wiener filter.

4.2 Surround inhibition

Next, surround inhibition reduces the strength of those edges which are surrounded by other edges. This mechanism is inspired by psychophysical and neurophysiological findings (see [7-9] and references therein). In [7-9] the contour strength $c(x,y)$ is computed by subtracting an inhibition term T_{σ} from the gradient magnitude, $M_{\sigma} = |\tilde{I}_{\sigma}|$:

$$c_{\sigma}(x,y) = |M_{\sigma}(x,y) - \alpha T_{\sigma}(x,y)|^+ \quad (15)$$

where the parameter α controls the strength of the inhibition.

The inhibition term T_{σ} is defined as the local weighted average of M_{σ} on an annular surround r around each pixel. Since T_{σ} is high on textured areas and low on isolated contours, texture can be suppressed without destroying object contours.

One drawback of this approach is that a contour in a given position is inhibited by other parts of the same contour that fall in the surround inhibition area of the concerned position. To solve this problem, we modify the definition of T_{σ} as follows: First, we split the annular surround r in two halves r^+ and r^- along the edge direction $\theta_{\sigma}(x,y)$ and exclude from these halves a band as shown in Fig. 5a. Second, we compute the inhibition term *after* non-maxima suppression.

Specifically, we first apply non-maxima suppression:

$$\tilde{M}_{\sigma}(x,y) = \begin{cases} \tilde{M}_{\sigma}(x,y), & (x,y) \in S_{\sigma} \\ 0, & (x,y) \notin S_{\sigma} \end{cases} \quad (16)$$

with:

$$S_{\sigma} = \left\{ (x,y) \left| \frac{\partial M_{\sigma}}{\partial u_{\sigma}} = 0 \quad \wedge \quad \frac{\partial^2 M_{\sigma}}{\partial u_{\sigma}^2} < 0 \right. \right\} \quad (17)$$

where u_{σ} is the direction of the gradient \tilde{I}_{σ} .

Then we consider the following pairs of orientation dependent filters $w_{\sigma,\phi}^{\pm}(x,y)$, which define two half-rings oriented along an angle $\phi \in$

$[0, \pi)$:

$$W_{\sigma,\phi}^{\pm}(x,y) = \text{DoG}_{\sigma}(x,y) \cdot U[\pm(x \cos \phi + y \sin \phi - a)] \quad (18)$$

$$w_{\sigma,\phi}^{\pm}(x,y) = \frac{W_{\sigma,\phi}^{\pm}(x,y)}{\iint_{\mathbb{R}^2} W_{\sigma,\phi}^{\pm}(x,y) dx dy} \quad (19)$$

where

$$|\xi|^+ = \begin{cases} \xi, & \xi \geq 0 \\ 0, & \xi < 0 \end{cases}, \quad U(\xi) = \begin{cases} 1, & \xi \geq 0 \\ 0, & \xi < 0 \end{cases} \quad (20)$$

and

$$\text{DoG}_{\sigma}(x,y) = \frac{1}{2\pi} \left| \frac{1}{(4\sigma)^2} \exp\left(-\frac{x^2+y^2}{2(4\sigma)^2}\right) - \frac{1}{\sigma^2} \exp\left(-\frac{x^2+y^2}{2\sigma^2}\right) \right|^+ \quad (21)$$

We compute the following two convolutions and take their minimum as an inhibition term:

$$\begin{cases} T_{\sigma}^{\pm}(x,y) = \left\{ \tilde{M}_{\sigma} * w_{\sigma,\phi}^{\pm} \right\} \Big|_{\phi=\theta_{\sigma}(x,y)} \\ T_{\sigma}(x,y) = \min\{T_{\sigma}^+(x,y), T_{\sigma}^-(x,y)\} \end{cases} \quad (22)$$

The convolutions are computed for a discrete set of orientations $\{\phi_i\}_{i=1}^{N_{\phi}}$, $\phi_i = \pi(i-1)/N_{\phi}$ and, for each pixel, we take the result obtained for the angle ϕ_i that is closest to the gradient orientation $\theta_{\sigma}(x,y)$.

On isolated edges (Fig. 5a), the local averages on both the sides are very low, ideally zero; consequently, $T_{\sigma}(x,y)$ is low and contours are not inhibited. On textured areas (Fig. 5b), the local averages on both the sides of an edge are high and similar to each other, thus the inhibition term is high and such texture edges are suppressed. Borders of textured areas are not inhibited, since $T_{\sigma}(x,y)$ is low on such points (Fig. 5c).

The advantage of performing surround inhibition after the non-maxima suppression is illustrated by Fig. 6. Fig. 6a shows the set S_{σ} of local gradient maxima and we see that the contours of the elephant are well separated from the rest of the texture. Therefore, a half-ring centred on a point of such a contour, and appropriately oriented, contains only a few nonzero pixels and the corresponding inhibition term T_{σ} will be extremely small. By comparing Figs. 6b and 6c we can see the improvement achieved by the proposed inhibition scheme with respect to [8, 9]. The proposed modifications allow the use of higher values of α , leading to more effective texture

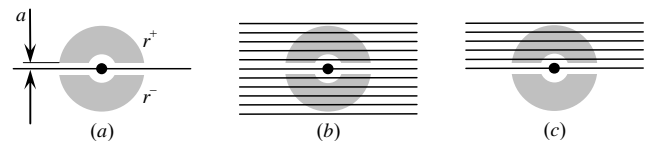


Figure 5 - Half-rings on which $M_{\sigma}(x,y)$ is averaged, for: (a) isolated edges, (b) textured areas, and (c) borders of textured areas.

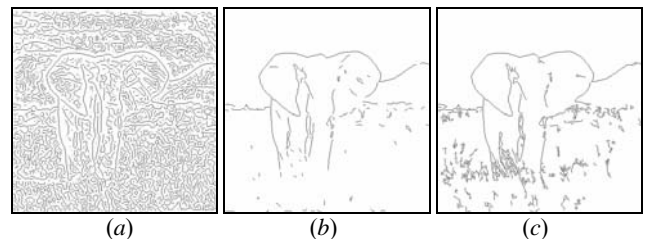


Figure 6 - (a) Set S_{σ} for the test image "Elephant". (b, c) Contours obtained with the inhibition schemes proposed in this paper (b) and in [9] (c).

suppression, without affecting object contours.

4.3 Binarization

Similar to other methods for edge and contour detection, the last step of the algorithm comprises binarization by thresholding. One well known problem with traditional thresholding techniques, such as global or hysteresis thresholding [1], is that they cannot deal with the quite common situation of weak contours. The gradient magnitude at such contours is smaller than at spurious edges originated by noise or texture. In this paper, we present a new thresholding algorithm, based on the observation that contours lead to long connected components of nonzero pixels, while texture edges lead to relatively short and thin components.

Let $\{C_k^{(\sigma)}\}_{k=1}^{N_s}$ be the connected components of S_σ (eq. 15), i.e.:

$$S_\sigma = \bigcup_k C_k^{(\sigma)} \quad (23)$$

For each connected component $C_k^{(\sigma)}$, we introduce a quantity $R_k^{(\sigma)}$, we call *contour weight*, defined as the sum of the values of $c_\sigma(x,y)$ over $C_k^{(\sigma)}$:

$$R_k^{(\sigma)} = \sum_{(x,y) \in C_k^{(\sigma)}} c_\sigma(x,y) \quad (24)$$

We define a binary map b_σ as the union of all connected components $C_k^{(\sigma)}$ whose weight $R_k^{(\sigma)}$ is above a given threshold t_R :

$$b_\sigma = \bigcup_{R_k^{(\sigma)} > t_R} C_k^{(\sigma)} \quad (25)$$

By comparing eqs. (23) and (25) we can see that $b_\sigma \subseteq S_\sigma$, where all components $C_k^{(\sigma)}$ which do not correspond to any meaningful contour have been removed (Figs. 6a, 6b).

On a weak edge, like the contour of the hill in Fig. 9a, the gradient magnitude $M_\sigma(x,y)$ is very low and it would (partially) not be detected by a standard binarization technique. However, since the contour of the hill forms a long chain of connected components, its weight $R_k^{(\sigma)}$ is high enough to survive the modified thresholding.

Therefore, thresholding the *global* contour weight $R_k^{(\sigma)}$ preserves the weak edges better than thresholding the *local* edge strength $M_\sigma(x,y)$ or $c_\sigma(x,y)$.

5. EXPERIMENTAL RESULTS

We now show and comment some examples of the results achieved with the proposed algorithm, both for noiseless and noisy images (SNR = 13dB), in comparison with four other existing algorithms (Figs. 7-10). As it can be seen, our approach (Figs. 7-10 b) gives the best results in terms of texture suppression, cleanness of the detected contours, and robustness to noise. Compared to the Canny edge detector [1] (Figs. 7-10 c), multiscale analysis, without surround inhibition [6], (Figs. 7-10 d) has some benefits: some texture is removed and noise is reduced. Comparable texture suppression is achieved with the single scale surround inhibition algorithm proposed in [9] (Figs. 7-10 e). The combination of multiscale analysis and surround inhibition [7] gives better results (Figs. 7-10 f). By comparing the results represented in Figs. 7-10 b and f, we can see the performance improvement achieved with the bilateral inhibition scheme and bayesian denoising proposed here: more texture is suppressed and the contours are cleaner, especially for the noisy images.

We carried out a quantitative performances evaluation by comparing

the results with a weighted multiset ground-truth drawn by hand. The ground truth associated with a given input image consists of a class $\{\mathcal{E}_i\}_{i=1}^{N_s}$ of sets of contour pixels. With each set \mathcal{E}_i a weight value γ_i is associated, corresponding to the importance attributed to the elements of \mathcal{E}_i . An example of such a ground-truth is given in Fig. 11, where the three sets $\mathcal{E}_1, \mathcal{E}_2, \mathcal{E}_3$, from the highest to the lowest value of γ_i , are represented by a thick, thin and dotted line, respectively. The dissimilarity between the ground truth and the output of a given operator defined as follows:

$$\rho = \frac{\sum_i \gamma_i EP_i}{\sum_i \gamma_i (EP_i + MP_i) + RT} \quad (25)$$

with:

$$\begin{cases} EP_i = \text{card}\{AR \cap \mathcal{E}_i\} & \text{Exact Points} \\ MP_i = \text{card}\{\overline{AR} \cap \mathcal{E}_i\} & \text{Missing Points} \\ RT = \text{card}\{AR \cap \bigcup_i \mathcal{E}_i\} & \text{Residual Texture} \end{cases}$$

where AR (Algorithmic Result) is the set of 1-pixels detected by a given algorithm, $\text{card}(X)$ indicates the number of pixels of the set X and \overline{X} indicates the complementary set of X . EP_i is the number of correctly detected contour pixels, i.e. the pixels present both in the result and in the ground truth. MP_i is the number of false negatives, i.e. points which are present in the ground truth but not in the operator output. RT is the numbers of points present in the AR but not in the ground truth and gives a measure of unsuppressed texture.

The values of ρ for the considered algorithms are presented in Fig. 12, where we can see that the proposed approach outperforms both standard techniques and more sophisticated algorithms based on single and multiscale surround inhibition.

6. CONCLUSIONS

The proposed multiscale contour detector, operating in the CHF domain, discriminates object contours from texture. At each scale, texture is suppressed by a biologically motivated surround inhibition step, where auto-inhibition is avoided by (i) the bilateral computation scheme of the inhibition term and (ii) the application of the inhibition after the non-maxima suppression. This allows to use a larger value of the inhibition coefficient and leads to more effective texture suppression.

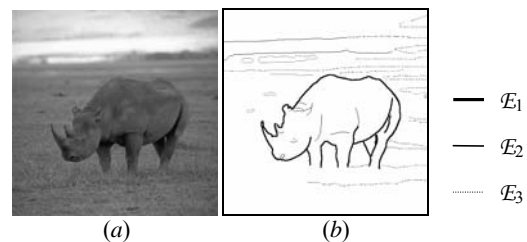


Figure 11 – Original image (a) and its multiset ground truth (b).

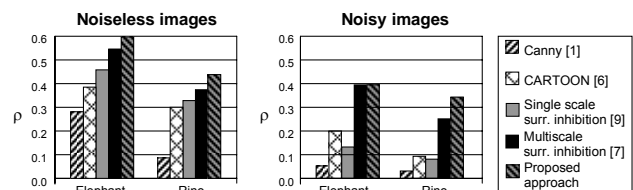


Figure 12 – Values of ρ for the studied algorithms, both for noiseless and noisy images.

Binary contour maps are obtained by thresholding the weight assigned to each connected contour component. This leads to better results than pixel-wise thresholding of the gradient magnitude M_σ because long weak edges are preserved. Robustness to noise for the general non-Gaussian case is achieved by using a Bayesian estimator. GSM models are employed for both the image and the noise and a closed form of the estimator has been provided.

As shown by the experimental results and performance evaluation, our algorithm outperforms both standard and more sophisticated approaches.

REFERENCES

[1] J.F. Canny, A computational approach to edge detection, *IEEE Trans. PAMI* 8(6), 1986, 679–698.
 [2] P.H. Gregson, Using angular dispersion of gradient direction for detecting edge ribbons, *IEEE Trans. PAMI* 15(7), 1993, 682–696.
 [3] G. Chen, Y.H.H. Yang, Edge detection by regularized cubic B-spline fitting, *IEEE Trans. SMC* 25 (4), 1995, 635–642.
 [4] T. Folsom, R. Pinter, Primitive features by steering, quadrature and scale, *IEEE Trans. PAMI* 20 (11), 1998, 1161–1173.
 [5] B. Julesz, “Visual Pattern Discrimination”, *IRE Transactions on Information Theory*, 8, 1962
 [6] W. Richards, H.K. Nishihara, B. Dawson, CARTOON: A

biologically motivated edge detection algorithm. MIT A.I. Memo No. 668
 [7] G. Papari, P. Campisi, N. Petkov, A. Neri, “A multiscale approach to contour detection by texture suppression”, *SPIE Im. Proc.: Alg. and Syst.* 2006, Vol. 6064A, San Jose, CA.
 [8] N. Petkov and M. A. Westenberg: Suppression of contour perception by band-limited noise and its relation to non-classical receptive field inhibition, *Biological Cybernetics*, 88, 2003, 236-246.
 [9] C. Grigorescu, N. Petkov and M.A. Westenberg: Contour detection based on non-classical receptive field inhibition, *IEEE Trans. on Image Proc.*, 12 (7), 2003, 729-739.
 [10] J. Portilla, V. Strela, J. Manwright, and E. P. Simoncelli, “Image denoising using scale mixtures of Gaussians in the wavelet domain,” *IEEE T-PAMI* 12(11), 1338–1351, 2003.
 [11] G. Jacovitti, A. Neri, “Multiresolution circular harmonic decomposition,” *IEEE Trans. on Signal Processing*, 48(11), 2000, 3242-3247 .
 [12] K.H. Liang, T. Tjahjadi and Y.H. Yang, “Bounded Diffusion for Multiscale Edge Detection Using Regularized Cubic B-Spline Fitting,” *IEEE Trans. SMC*, 29(2), 1999, 291-297.
 [13] A. Ding, A. Goshtasby, “On the Canny edge detector,” *Pattern Recognition*, 34, 2001, 721-725.
 [14] J. G. Daugman, “Six formal properties of two-dimensional anisotropic visual filters: Structural principles and frequency/orientation selectivity,” *IEEE Trans. SMC*, 13, 1983.

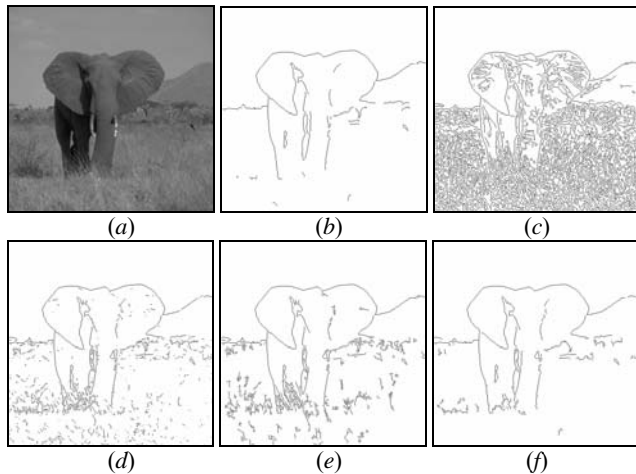


Figure 7 - (a) Input image “Elephant” and contours detected with: (b) the proposed approach, (c) the Canny edge detector, (d) the multiscale edge detector CARTOON without surround inhibition [6], (e) single [9] and (f) multi scale surround inhibition [7].

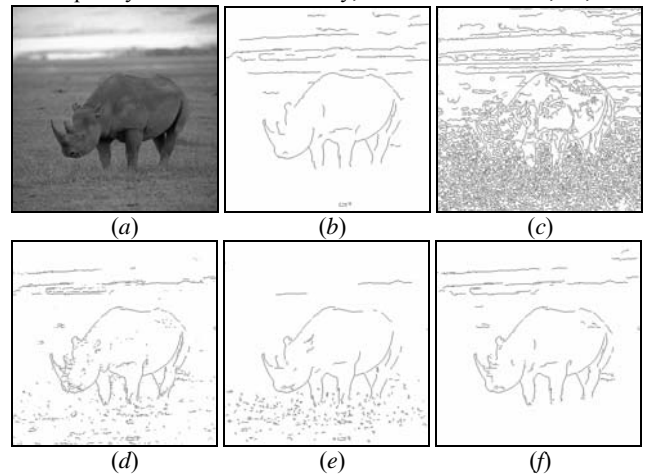


Figure 9 - (a) Input image “Rino” and contours detected with: (b) the proposed approach, (c) the Canny edge detector, (d) the multiscale edge detector CARTOON without surround inhibition [6], (e) single [9] and (f) multi scale surround inhibition [7].

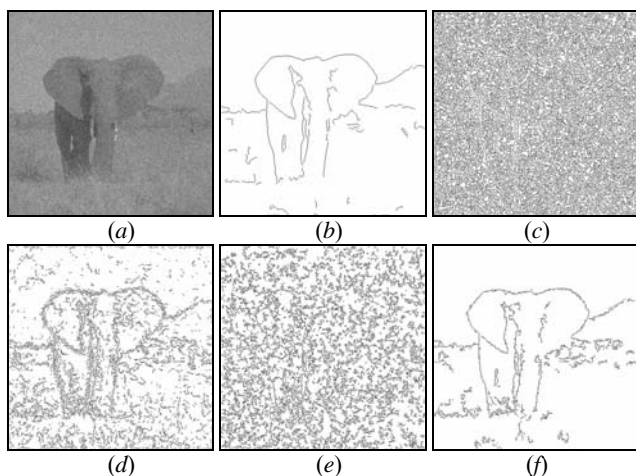


Fig. 18. Contours detected on the noisy image test (SNR = 13dB)

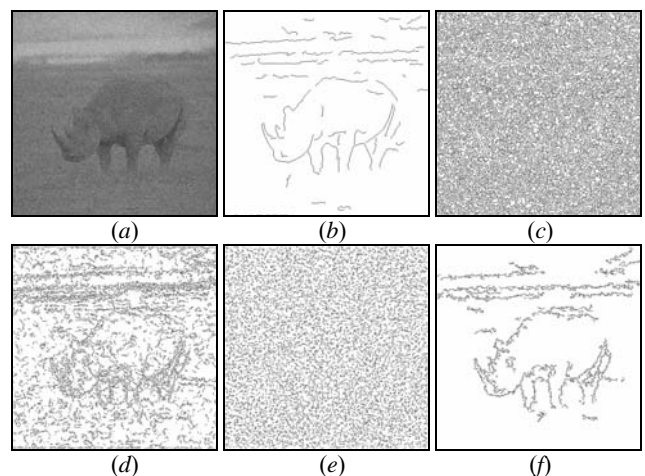


Fig. 10. Contours detected on the noisy image test (SNR = 13dB)